Title

Microfluidic cap-to-dispense (μCD): a universal microfluidic—robotic interface for automated pipette-free high-precision liquid handling

Journal

Lab on a Chip, 19(20)

ISSN

1473-0197

Authors

Wang, Jingjing

Deng, Ka

Zhou, Chuqing

et al.

Publication Date

2019-10-09

DOI

10.1039/c9lc00622b

Peer reviewed

HHS Public Access

Author manuscript

Lab Chip. Author manuscript; available in PMC 2020 October 09.

Published in final edited form as:

Lab Chip. 2019 October 09; 19(20): 3405–3415. doi:10.1039/c9lc00622b.

Microfluidic Cap-to-Dispense (μCD): A universal microfluidic-robotic interface for automated pipette-free high-precision liquid handling

Jingjing Wang[§,a,b], **Ka Deng**[§,a], **Chuqing Zhou**[§,b], **Zecong Fang**[b], **Conary Meyer**[b], **Kaustubh Umesh-Anjali Deshpande**[b], **Zhihao Li**[c], **Xianqiang Mi**[d], **Qian Luo**[e], **Bruce D. Hammock**[f], **Cheemeng Tan**[b], **Yan Chen**[a], **Tingrui Pan**[b]

[a]Institute of Biomedical and Health Engineering, Shenzhen Institutes of Advanced Technology, Chinese Academy of Sciences, Shenzhen, 518055, China

[b]Department of Biomedical Engineering, University of California, Davis, California, 95616, USA

[c]Department of Computer Science, Columbia University, New York, New York, 10027, USA

[d]Laboratory of System Biology, Shanghai Advanced Research Institute, Chinese Academy of Sciences, Shanghai, 201210, China

[e]Institute of Biomedicine and Biotechnology, Shenzhen Institutes of Advanced Technology, Chinese Academy of Sciences, Shenzhen, 518055, China

[f]Department of Entomology and Nematology and UCD Comprehensive Cancer Center, University of California, Davis, California, 95616, USA

Abstract

Microfluidic devices have been increasingly used for low-volume liquid handling operations. However, laboratory automation of such delicate devices has lagged behind due to the lack of world-to-chip (macro-to-micro) interfaces. In this paper, we have presented the first pipette-free robotic-microfluidic interface using a microfluidic-embedded container cap, referred to as a Microfluidic Cap-to-Dispense (μCD), to achieve a seamless integration of liquid handling and robotic automation without any traditional pipetting steps. The μCD liquid handling platform offers a generic and modular way to connect the robotic device to standard liquid containers. It utilizes the high accuracy and high flexibility of the robotic system to recognize, capture and position; and then using microfluidic adaptive printing it can achieve high-precision on-demand volume distribution. With its modular connectivity, nanoliter processability, high adaptability, and multitask capacity, μCD shows great potential as a generic robotic-microfluidic interface for complete pipette-free liquid handling automation.

[§]These authors contributed equally to this work.

Conflicts of interest

There are no conflicts to declare.

Introduction

Liquid handling is an essential step involved in almost all laboratory procedures for contemporary life sciences and medical studies. These include polymerase chain reaction (PCR), immunoassays, and drug screening; where biological or clinical samples have to be freq uently transferred between storage containers or dispensed onto analytical substrates.[1,2] With the new advent of precision and personalized medicine, the demand for handling minute volumes of samples has increased drastically. For instance, a large array of combinatorial assays often have to be prepared and screened with sensitive and precious samples in synthetic biological studies[3–5] and combinatorial drug therapies[6,7]. In these studies traditional manual procedures of liquid handling using micropipettes is cumbersome and impractical.[8] To minimize analytical errors and improve the operational efficiencies, further technical advancement is essential for liquid handling methods with higher precision, lower volume processing capacity, and negligible human-induced errors and interruptions.[9–11]

To overcome the human errors involved in the traditional manual operations, an array of automated liquid handling workstations have been developed in the last couple of decades to resemble the pipetting function using a robotic interface.[12–14] In general, piston-driven single channel or multichannel micropipettes are mounted onto a high-precision 3-axis traveling stage (e.g., Fluent™ from Tecan and OT-2™ from Opentrons), which directs the spatial movements and positioning, and can be programmed to automate a number of repetitive protocols and workflows, resembling the manual pipetting procedures.[15,16] Benefiting from the rapid development of industrial robots, the concept of co-robots has been recently introduced with the purpose of laboratory automation. The idea is to offer more flexible and adaptive operations compared to their existing counterparts. These labor-saving robotic devices aim to improve the productivity and throughput of routine and repetitive work, while offering the capacity to work with laboratory personnel and research staff side-by-side. These processes will be accompanied by injury preventing sensors and embedded protocols.[17] A new variety of pipetting-manipulating co-robots have been devised and added to the family of liquid-handling equipment, such as Mantis from Formulatrix and ReadyGo from BioWavelet.[18,19]

Although encouraging progress has been demonstrated by adopting robotic automation to liquid handling in both industry and academia, one major limitation of this approach remains inadequately addressed, namely the accuracy of low-volume (sub-microliter) processing. Moreover, the intrinsic differences between human-pipette and machine-pipette interfaces have been largely overlooked, aside from marginal modifications, thereby creating further barriers to automate additional human-centric operations.[20–22] Additionally, to address such a growing demand in ultralow-volume liquid handling, nanoliter or picoliter dispensing technologies have been quickly adopted from the inkjet printing industry.[11,23–25] While the pipetting method always results in a residual volume on the pipette tips and leads to inaccuracy in a low-volume setting, inkjet printing is able to eject liquid from a small orifice by utilizing a precisely-controlled driving force to overcome the surface tension and ensure accuracy of liquid volumes.[2,26,27] Both the do-it-yourself method by modifying from an off-the-shelf inkjet printer (e.g., PIXMA iP1300 from Canon, and K100 from EPSON)[28–30] and

the commercial solutions of a high-precision dispenser (e.g. Dimatix from Fujifilm, and D300 from Tecan)[31–34] have become widely employed in sub-microliter dispensing. However, the existing high-precision dispensing nozzles either require an expensive integrated piezoelectric actuator to achieve the dispensing precision, which typically involves complicated manufacturing process,[35] or relies on a thermal expansion approach, which is incompatible with many biological systems.[10] Additionally, these high-cost dispensers prohibit their application for disposable uses, and cumbersome washing and cleaning is required to minimize cross-contamination between uses.[9,36] Moreover, the connection to the dispenser head is rather conventional, using extensive classical tubing and fitting connections, resulting in large loading and dead volumes, considerable waste of precious reagents, and difficulties when changing reagents and samples.[27,37,38] Meanwhile, ultralow-volume liquid handling could also be realized by pneumatic drive. Miniature droplets could be generated by pulsed pneumatic pressure. The frequency of pulse waves in the droplet generator can be tunable by the pulse duration, nozzle size and driving pressure.[39] The pneumatic valve implemented next to the microfluidic T-junction can produce arrays of uniform emulsion droplets in various sizes in a high throughput manner.[40] In our previous studies, we have shown that pneumatic droplet generation method has great potential in biological and chemical studies, since the droplets size could be highly controllable using the tunable geometrical and pneumatic parameters.[41,42]

Recently, microfluidic-derived dispensing technologies, also known as microfluidic adaptive printing (MAP), have been established to generate picoliter and nanoliter droplets on-demand. By separating the actuating mechanism from the liquid-containing cartridge, the microfluidic printing has the advantages of simple fabrication, inexpensive construction, non-contact dispensing, and flexible multiplexing, allowing a low-cost alternative to existing nanoliter dispensing solutions.[43] In our original work on MAP, we have designed and fabricated an interchangeable microfluidic cartridge with multiplexed sample channels, driven by a dot-matrix printer head, featuring a low loading volume of 0.6 μL and a dead volume of 0.05 μL.[9,44] By utilizing both piezoelectric and pneumatic drives, MAP printing achieves linear scalability, high frequency, and tunable droplet generation. It has been successfully employed in multi-parametric gene regulatory studies and combinatorial peptide microarray synthesis.[5,38,41,42,45] More recently, several high-precision sub-microliter pipetting systems using the MAP mechanism have been introduced with disposable microfluidic pipetting tips.[22,46–48] Although existing studies have illustrated the potential of integrating microfluidic printing with a commercial micropipette to achieve high precision and on-demand nanoliter volume dispensing, the functions of such devices are limited to dispensing only, while the interface between the machine and the pipette tips remains unchanged. Therefore, the lack of world-to-chip (macro-to-micro) connectivity still prevents complete automation.

In this study, we introduce the first pipette-free robotic-dispensing interface using a microfluidic-enabled container cap, referred to as a Microfluidic Cap-to-Dispense (μCD) which achieves a seamless integration of liquid handling and robotic operations. The new pipette-free microfluidic-robotic interface offers a simple and modular way to connect the robotic drive with a standard liquid container, exploiting the high accuracy and high flexibility of the robotic recognition and motion system to achieve high-precision on-

demand volume dispensing by microfluidic adaptive printing. In brief, this novel microfluidic liquid-handling system includes multiple functions for laboratory automation in a complete automated solution, namely target/sample recognition, container catch-and-release, positioning, high-precision dispensing, and multiplexing. As the core of the μCD concept, the multilayer-assembled microfluidic cap consists of a microfluidic printing nozzle, a tube connector, and two pneumatic control channels reversibly linked to the robotic effector upon contact. In addition, the robotic effector has been custom-modified to grab the liquid container, but also contains the pneumatic drive to power the microfluidic cap through the contact interface. As a demonstration, we have employed the μCD system to fully automate the characterization of a synthetic genetic circuit, in which multi-dimensional analyses of two regulatory factors have been investigated in high throughput with low consumption of reagents, yielding an optimized condition for the selected genetic expression process. This experiment can be easily modified and adapted to similar combinatorial biological processes. Compared with serial dilutions typically operated by manual pipettes in most biological labs, our system improves the efficiency and accuracy of multifactorial studies with a wide range of concentrations. With its modular connectivity, nanoliter processability, high adaptability, and multitask capacity, μCD has shown a great potential as a generic robotic platform for future pipette-free laboratory automation.

Principle

The μCD system is designed to establish a universal interface between robotic automation and liquid handling of chemical and biological solutions without involvement of traditional micropipetting processes.[1] It comprises of four essential components: the microfluidic dispensing cap, the robotic end-effector with pneumatic connectors, the robotic arm/motion stage, and a machine vision unit for recognition, as shown in Fig. 1a.

As the key component, the microfluidic dispensing cap has been fabricated by stacking three polymer layers from bottom to top: a membrane layer with a high-precision micro-machined nozzle, a microfluidic channel layer, and a 3D-printed fitting adapter. The micro-machined nozzle plays an important role in determining the process for droplet pinch-off and ejection, while the microfluidic layer balances the discrete output of droplets and constantly refills the fluid. Moreover, the custom 3D-printed adapter is intended to fit and connect to standard liquid containers with various sizes in a regular lab setting, but also incorporates all liquid and pneumatic connections, such as a channel towards the microfluidic layer, another tube connected to the enclosed solution, along with two additional pneumatic channels that can be reversibly linked to the robotic end-effector upon contact.

Notably, the classic robotic end-effector, a parallel-styled gripper with two fingers, is equipped with a rubber contact pad on each finger to catch the microfluidic dispensing cap with the pneumatic channels, as illustrated in Fig. 1a–b. The elastic pads made of rubber resin have been embedded in the pneumatic connections using O-ring seals. Upon contact, the compressed air from the programmable pneumatic drive can be directed towards the microfluidic dispensing cap to refill and dispense the droplets from different channels with a millisecond resolution. A 4 degree-of-freedom robotic arm has been combined with the end-effector to enable automated manipulations. An expanded IO on the robotic arm has been

utilized as a communication means to coordinate and synchronize the functions, such as movement, catch-and-release, and dispensing.

The machine vision module achieves two functions. The first is to recognize the container information encoded by a QR code on the side of the cap, and the second is to use the QR code as reference coordinates and to help position the dispensing cap for further operations. Specifically, when guided by the machine vision, the robotic arm first identifies and locates the container with the targeted reagent using the QR code. Consecutively, the end-effector (gripper) is commanded to engage into the two opposite sides of the microfluidic cap with pneumatic connections established.

As depicted in Fig. 1b, the droplet printing process is controlled and propelled by two external pneumatic drives: a low-pressure source (P_L) to load the liquid from the container to the dispensing nozzle and a pulsed high-pressure one (P_H) to eject droplets from the nozzle. Fig. 1c–d illustrate simplified hydraulic circuits to describe the two states of the droplet dispensing process labeled with major influential parameters, namely a loading/refilling state (Fig. 1c) and a dispensing state (Fig. 1d). In particular, the fluid dynamics inside the microchannel can be modeled as a constant displaced flow caused by the continuous input of refilling liquid and the dispensing output of discrete droplet volumes. The displaced flow moves through the microchannel, with flow resistance of R_c, towards either the nozzle openings with flow resistance of R_n or the adjacent side channel with flow resistance of R_r. At the interface between the side channel and the robotic effector, a one-way valve is attached to prevent the fluid from leaking into the pneumatic drive.

During the refilling state, liquid from the container will fill out the microfluidic cap while stopping at the dispensing nozzle and the robotic interface with the one-way valve, both of which can be modelled as fluidic diodes D_n and D_r, respectively, as shown in Fig. 1c. As the refilling pressure P_L is smaller than either the valve-opening pressure or the Laplace pressure of the nozzle, the liquid will reach an equilibrium state after filling up the dispensing cap. Once a high pulse pressure P_H is applied from the side channel during the subsequent printing state, a droplet with a volume of V is ejected through the nozzle opening with a volumetric flowrate of Q, as shown in Fig. 1d. The following equation expresses the relationship between the dispensed droplet volume (V) and the flow resistance of the microfluidic channel and the nozzle opening along with the pneumatic drives:

$$V = Q \cdot T = \frac{P_H/R_r + P_L/R_c}{1/R_r + 1/R_n + 1/R_c} \cdot \frac{T}{R_n} \approx \frac{P_H \cdot T}{R_n} = \frac{P_H \cdot T \cdot \pi r^4}{8\mu t} \quad \text{(Eq. 1)}$$

where T is the duration of the pulsed pressure, r is the nozzle radius, t is the nozzle thickness and μ is the dynamic viscosity of the liquid. Notably, in the dispensing cap design, we apply a design rule to keep $R_r << R_n << R_c$, which further simplifies the equation. Within the laminar flow region, the flow resistance of the nozzle R_n follows the classic Hagen-Poiseuille equation[49].

It is also worth noting that the capacitance has been ignored in the figure 1c and d. Since the liquid-containing vessels (including the EP tube, the connecting tubings and the μCD chip) are all relatively rigid, the air pressure in the refilling end is constant, and the dead volume/air compressibility inside the tubing from the printing end is minimized, so that we can ignore the hydraulic and pneumatic capacitances.

In addition, the liquid inside the EP tube has a hydrostatic pressure (0.014 psi) that's much smaller than the refilling pressure P_L (0.5 psi) and therefore the influence of the height change inside the EP tube is negligible; The liquid inside the EP tube can be modelled as a variable resistor, with a changing resistance as the height of the liquid varies. However, the resistance is found much smaller than R_c and therefore is also neglected in our simplified circuit.

Experimental methods

Design and fabrication of the microfluidic cap

A UV-laser (JG15S, Zhengye Laser, China) was used to ablate a PMMA membrane to form nozzles. The laser ablation parameters were optimized to achieve a uniform edge of the circular though hole, resulting in a vertical pinch-off process for droplet generation with rare satellites scattering on the substrates and rare droplets adhering to the nozzles. Micro-circles with radius of 5, 15, 25, 35, 45 and 55 μm were designed using CAD software and produced ablated nozzles with radius of 25, 32.5, 40, 50, 62.5, and 75 μm, by shrinking the PMMA material (thickness: 75 μm) at a high temperature. The UV-laser was also used to ablate a double-side membrane (ARcare® 90445, Adhesives Research, thickness of 80 μm) to form microchannels with a width of about 800 μm. The milli-chip was designed in SolidWorks software and fabricated with a photosensitive resin using a 3D printer (Shenzhen WeNext Technology Co., Ltd), with 1 mm-diameter inlets and outlets.

The microfluidic dispensing cap consists of three polymer layers: a membrane layer with a high-precision micro-machined nozzle, a microfluidic channel layer, and a 3D-printed fitting adapter. The micro-chip layer was firstly stuck onto the top of the milli-chip, with microchannel ends aligned to the two openings on the bottom surface of milli-chip for liquid refilling and output, respectively. The nozzle layer was then stuck onto the microchip, with nozzle precisely aligned to the end of the microchannel for liquid dispensing. Subsequently, a steel needle (1 mm diameter, 1.2 cm length) was inserted into the center hole of the plug part of the milli-chip.

Particularly, the two through-holes have been designed on the two sides of the cap to connect the pneumatic driving channels and the robotic end-effector upon capture, the third center-through-hole connected to the steel needle (1 mm diameter, 1.2 cm length) is for liquid transferring from EP tube to micro-chip.

Then the fabricated microfluidic caps were inserted into standard liquid containers, such as 200 μL EP tubes. Liquid reagent flows through the needle, microchannel and nozzle, then upward to another side-through-hole and stops at the one-way valve. Pneumatic pulse

pressure then goes through the valve and pushes the liquid toward the microchannel and nozzle, as shown in the enlarged illustration in figure 1b.

The nozzle and microchannel were designed to have a high resistance for precise droplet volume control. After the droplets are pinched off under the nozzle, the residual liquid is retracted backwards into the microchannel, driven by its Laplace pressure[50], while the microchannel balances the discrete output of droplets and constantly refills the liquid. The displaced flow moves through the microchannel either upwards to the pulse source or downwards to the nozzle. When the pulsed air pressure is switched on and off, the extra volume of fluid is ejected through the nozzle opening, not backward into the microchannel due to its high resistance $R_c >> R_n$.

Calibration and imaging methods

Planar PDMS membranes coated on glass-slide substrates were used as the calibration surface to characterize the volumes of the printed aqueous droplets. Since the contact angle of bare PDMS is close to 90 degrees, it offered a simple method to calculate the volume of these hemispherical droplets. To decrease the evaporation rate, dimethylsulfoxide (DMSO) was added to the aqueous solution with a mixing ratio of 2.5: 23.75: 73.75%, color dye: DMSO: deionized water. The images of droplet dispensing process are imaged by a high-speed camera (VEO-E310L, Phantom, USA). To characterize the dispensing parameters, arrays or patterns of droplets were deposited onto the PDMS surface. The images of the droplets were captured with a standard optical microscope (EVOS XL, Life Technologies, USA) and analyzed using the imageJ software.

System integration and patterning algorithm

To introduce a pneumatic drive into the microfluidic dispensing cap, a robotic end-effector, more specifically, a parallel gripper with two fingers, applies a horizontal force to tightly hold the cap. A pair of customized 3D-printed air connectors with holes in the center surrounded by silica rubber O-rings with a diameter of 2 mm, were mounted on both gripper fingers to introduce compressed air into the cap and guarantee a seamless pneumatic connection as a plug-and-play interface. The compressed air from the programmable pneumatic drive can be precisely controlled and actuated into the two opposite sides of microfluidic cap for accurate refilling and dispensing with sub-millisecond resolution, resulting in the formation of nanoliter droplets. In the pneumatic system, we have included a custom-made circuit based on Arduino architecture and two mini solenoid valves (LHDA1221111H, Lee Co). The pressure pulses have been derived from a pressure regulator (OBKZN) with a range up to 15 psi and a precision of 0.01 psi connected to the compressed air from an air compressor.

To precisely position the droplet in the right place, translational motions were needed for the dispensing task, usually described in a Cartesian coordinate system. A 4-DoF robotic arm was used to achieve this demand, in which three DoFs on the base, the upper arm and the lower arm were programmed to approach the target position in XYZ coordinate system and the last wrist rotational DoF was used to adjust the orientation (of the cap) around the Z-axis.

The robotic end-effector and the arm were combined to form a manipulator, whose functions were coordinated and synchronized with the other parts of the system via the expanded IOs on 5 V TTL-level and 3.3 V LVTTL-level as communication means.

The desired complicated patterns were designed in advance as pixel matrices. On each pixel, the type of the reagent and the droplet count were designated. For each reagent, there will be a matrix, where the value of each element, a natural number, specifies the droplet count. The droplet count can vary from zero to several tens, resulting in a blank spot at a distinct drop. After catching a target reagent from the designated position, the robotic manipulator will move and stay at the printing region and execute the printing task instructed by the corresponding pattern matrix. The stay period was also determined by the droplet count in this position. By providing multiple reagents and their pattern matrices, objects can be mixed in each specified position. The spatial interval of the droplets between the adjacent elements in the pattern matrix was adjustable in the program of the robotic manipulator. Often, the interval was set above 0.5 mm to prevent contamination from adjacent droplets. The mechanical oscillation of the robotic arm in this report is on the order of a few hundred milliseconds. Presently, consecutive dispensing at the same place is not disturbed by the oscillation, and the shortest interval of two consecutive dispensing at adjacent points is approximately 500 ms, including the settling time for the oscillation. By upgrading it to a higher-end robotic arm, this interval can be reduced to be smaller. The presented system enables automated precise dispensing of liquid and reagents in modern complex lab dispensing tasks, such as large-scale complicated pattern in multi-well plates.

Biomolecular micropatterns demonstrations

To demonstrate the compatibility of the μCD system with biological samples a multiparametric dose response experiment was conducted. This experiment consisted of 3 components: bacteria, isopropyl β-D-1-thiogalactopyranoside (IPTG), and Luria Broth (LB). The bacterial strain used in this paper was generated by cloning the fluorescent protein mCherry into the pET15b plasmid and transforming it into *E. coli* BL21 (DE3)-pLysS cells (Novagen). Overnight cultures were made from fresh colonies of that strain. The cultures were then diluted in fresh media 2 hours prior to printing allowing them to reach a concentration of approximately 10^8 cells/mL. All of the reagents were then sequentially printed to build each unique reaction.

The droplets were dispensed onto PDMS-coated cover glass to allow for observation on a Nikon Eclipse Ti-E inverted microscope. A 2 mm-thick layer of mineral oil was added after printing to cover the droplets to avoid evaporation. A Texas red filter cube (560 nm excitation/630 nm emission) from Nikon was used to measure the mCherry fluorescence. Images of the droplets were automatically taken over several hours. The fluorescence intensities in the images were then analyzed using ImageJ and Matlab scripts. The half maximum effective concentration was calculated by determining the inducer concentration required to achieve half the maximal fluorescence for each cell density and then averaged.

Results and discussion

Automation of the μCD platform

A complete μCD operation flow includes multistep automation, i.e., sample recognition, catch, positioning, dispensing, return and release, as illustrated in Fig. 2.

As aforementioned, the target identification has been achieved through the machine vision using a QR-code recognition algorithm (Fig. 2a). In addition, the QR-code recognition has provided the robotic arm with spatial coordinates to allocate and capture the targeted containers. The robotic gripper with two fingers grabs the microfluidic dispensing cap with the pneumatic link established (Fig. 2b). Following the container capture, the robotic arm moves the c-equipped container to the target position and starts to dispense the liquid driven by the programmed pneumatic control (Fig. 2c). After delivering the desired volume, the robot returns the container back to the original location (Fig. 2d), while it is ready to start another cycle of dispensing (Note: The operational videos of the automated μCD have been included in the ESI).

Characterization of droplet dispensing

The Coefficients of Variation (CVs) have been considered to evaluate the consistency and distribution of the single droplet volumes printed from the μCD system. Fig. 3a shows a microscopic image of a printed droplet array on a planar surface from a 25% DMSO solution (with a viscosity of 1.5 cP and surface tension of 55.4 mN/m at 25 °C).[51,52] Furthermore, the printed single droplet array with the targeted volume of 84 nL have been measured and plotted in Fig. 3b. Computed from the droplet diameter measured by the histogram plotted by ImageJ, it shows a mean value of 84 nl and a diameter CV of 3.18%, confirming the high repeatability of the single droplet printing of the μCD system. Furthermore, the CVs of the printed droplet sequences have then been evaluated by repetitive dispensing of 100 to 1000 times, with the single droplet volume targeted at 100 nL. The weights of these printed volumes have been assessed by a high-precision scale and summarized in Fig. 3c, where the x-axis represents the targeted volumes while the y-axis stands for the corresponding volumes measured by the gravitational method. As can be seen, the measurement results, based on three-time repeats, have been plotted and fitted into a linear curve, exhibiting a high correlation coefficient of R^2 =0.9994. In Fig. 3a–c, the experiments have been conducted under the same condition of the pulse pressure of 3.0 psi and pulse duration of 6 ms, with nozzle radius of 40 μm.

For a classic EP tube with capacity of 200 μl, the current μCD design could continuously produce more than 3000 droplets with each loading with 80 μm nozzles, or 9000 droplets with 65 μm nozzles, till the last drop of reagent in the container. This could be highly desirable for the precious biological/chemical reagents. The customized pattern of such has been automated by the robotic arm, by which the positioning precision and spatial resolution are mainly determined.

As expressed in Eq. 1 of the microfluidic printing model, a number of potential parameters can influence the droplet formation process, including nozzle radius and thickness, fluidic viscosity, pulse pressure and duration.[44,53] In this study, we have chosen the major

influences of the nozzle radius (r), the pneumatic pressure (P_H) and the pulse duration (T) to be experimentally assessed.

First of all, the nozzle dimension (r) plays an important role in determining the droplet volume.[35] A range of different nozzle radius with the same milli- and micro-chips have been investigated with the droplet variations in response to the driving pulses. As shown in Fig. 3d, given a fixed pulse pressure of 3.0 psi and pulse duration of 6 ms, the ejected droplet volume increases in an approximately linear fashion from 38 nL to 291 nL with the nozzle radius rising from 32.5 to 75 μm, that is 7-fold volume expansion. As expected, when the nozzle size keeps small, the experimental data match well with the inverse 4th-power relationship between the droplet volume and nozzle dimension, as can be theoretically predicted by Eq. 1. However, as the nozzle size increases (above 60 μm in radius), the original assumption of $R_r << R_n$ becomes no longer valid, and therefore, the experimentally measured values deviate from the theoretical predication of the desired droplet volume by a large margin. These deviations become more severe in a larger nozzle (up to 67% in the nozzle radius of 75 μm) as shown experimentally.

Further reducing the nozzle dimension would result in drastic decrease in the droplet size; meanwhile, it causes the nozzle resistance to hike considerably. However, in order to eject the fluid out from the nozzle using the MAP principle, it requires the nozzle resistance R_n to be considerably lower than that of the microchannels R_c. We have experimentally determined that the minimal nozzle radius would be greater than 25 μm for effective printing in the μCD platform. On the other hand, a wider nozzle would lead to larger ejected droplets, while the maximal refilling speed of the liquid sample is directly proportional to the microchannel resistance, and caped at about 300 nL/s in the system, given the refilling pressure of 0.5 psi and pulse duration of 20 ms.

Besides the nozzle geometry, the pneumatic drive pressure (P_H) can also be determinant in the droplet formation, as the model predicts (Fig. 1b). We have investigated the influences from the magnitude and pulse duration of the pneumatic drive, respectively. Fig. 3e illustrates the experimental results of the droplet volumes at multiple pressure levels, given a fixed pulse duration. As evident by a well-fitted measurement curve, the rising volume of the ejected droplets is nearly linearly correlated with the elevating pulse pressure. In particular, by extending the pneumatic pressure from 2.0 psi to 6.0 psi, the droplet size has been scaled with more than 2-fold increment from 23 to 58 nL with 32.5 μm nozzles, and 60 to 145 nL with 40 μm nozzles, at the fixed pulse duration (of 6 ms). It is worth noting that a minimal pressure (of 2.0 psi) becomes necessary to overcome both the internal resistance of the microchannels and Laplace pressure presented at the nozzle for the droplet formation.[50] Moreover, Fig. 3f shows a similar linear relationship between the pulse duration and the droplet volume, ranging from 21 to 55 nL with 32.5 μm nozzles, and 57 to 143 nL with 40 μm nozzles, at the fixed pulse pressure (of 3.0 psi). In principle, a shorter pulse duration would lead to faster droplet ejections, and thus, a higher dispensing speed. However, the restrictions have been presented by both the mechanical response time of the solenoid valve (~2 ms) and the response time of the compressed air pressure inside the channel, from which a minimal pulse duration of 3 ms is resulted. In conclusion, the droplet sizes can be fine-

tuned by either the geometrical parameter of the nozzle (i.e., its radius) or the on-demand pneumatic drive pressure (i.e., the pressure level and duration).

Demonstrations of the μCD platform

As discussed above, the μCD dispensing platform would enable the complete lab automation solution with high throughput and low reagent consumption for various biological and clinical procedures. As proof-of-concept experiments, we have established collective patterns of monochrome or multi-colored droplets to images of combinational arrays, as shown in Fig. 4. It includes a planar molecular pattern with single and multiple droplet dispensing (Fig. 4a); a Taiji pattern (Fig. 4b) and an Eiffel tower shape (Fig. 4c) with two different colors printed from separate μCD containers; a multicolor DNA helix structure, with strangled chains presented by two types of 5-in-1 droplets (red and light blue dots) and A/T/C/G by multicolor single droplets (pink, green, yellow and purple), respectively (Fig. 4d); a world map formed by an array of 985 single droplets (Fig. 4e); and a multicolor 3-in-1 droplets array to form logos of the UC DAVIS and SIAT CAS (Fig. 4f). The multiplexed and combinatorial pattern formation illustrates the automated multi-reagent processing capability. As each dispensing, μCD container with cap is independent and modularized, the entire robotic operating system can be easily expanded to large-scale multi-reagents dispensing applications, without a limited number of reagents.

To demonstrate the compatibility of the μCD system with biological sample processing, we implemented a generic combinatorial experiment utilizing three different reagents to assess their interactions. The components included a strain of bacteria with an inducible genetic circuit, an inducer, and a diluent. The objective of this experiment was to characterize the response of the genetic circuit at various concentrations against a range of inducer concentrations. Such experiments are required when constructing complex genetic systems[54], assessing the efficacy of a drug on a system[44], and optimizing component stoichiometry in a variety of reactions[38,55].

Here, we studied the response of a LacI repressible genetic circuit, which would give rise to the expression of the fluorescent protein mCherry upon sufficient induction by its inducer, isopropyl β-D-1-thiogalactopyranoside (IPTG). To achieve this, a 10-fold range of concentrations of both the bacteria and the inducer were tested in one hundred independent reaction conditions in which each spot contained 18 ejections, leading to 1.2 μL in total. To ensure the dispensing accuracy of the proposed biological experiment, a 10 ×10 array of combinatorial mixtures comprised of 3 color dyes were first generated using the μCD system as shown in Fig. S2a, followed by the dispensing the biological samples and reagents (in Fig. S2b).

As a result, the two-dimensional combinatorial matrix of the cell suspension and inducer assay was established. Fig. 5a and b show the fluorescent images taken from the combinatorial droplet array, at 3 and 5 hours, respectively. To quantify these images, the total fluorescent densities were measured and normalized as shown in Fig. 5c and d. with ranges of [−0.1, 0.1] and [−1, 1] respectively. From this data, we determined the half maximal effective concentration (EC_{50}) of IPTG to activate the circuit to be around 66.7 μM. The EC_{50} determined by this experiment is consistent with previously reported

characterizations of similar genetic circuits.[56,57] This experiment also demonstrates printing of sensitive reagents, which if exposed to harsh conditions will cease to work. The μCD also demonstrates its ability to limit cross contamination between reagents as no fluorescence is observed in droplets without cells or inducer. Several concerns could be taken into consideration regarding the risk of sample adhesion to the tube. First of all, in comparison with the standard pipetting system, the needle was inserted into the end of the EP tube in the μCD system, and thus, the majority of the liquid sample could be directed to the dispenser by the continuous pneumatic drive. As a result, the dead volume could be substantially reduced. Secondly, similar to the pipette tips, the microfluidic caps are intended for only single use once the reagents or samples depleted inside, which eliminates the cross-contamination concern. Risks could present when biomolecules adhere to the container, tubing, microchip surfaces, and alter the concentrations and the viscosity of the solution. However, in our biological studies, the fluorescent protein expression profile has been observed consistently with what has been reported in standard expression experiments conducted in test tubes. In summary, compared with the manual dilution processes operated in many biological labs, our μCD system offers a fully automated pipette-free solution with considerable improvement in efficiency and accuracy of multifactorial studies, while completely liberating laboratory personnel from repetitive and routine pipetting work with human-induced errors and interventions eliminated.

Conclusions

In this paper, we have developed a pipette-free microfluidic cap-to-dispense method, employing a microfluidic cap with seamless plug-and-play connectivity to robots. It allows automatic high-precision sample dispensing ranging from nano-liter to micro-liter volumes, directly from standard biological containers, without involving any pipetting transfer and potential cross-contamination procedure. As a paradigm-shifting platform, this μCD robotic liquid handling system offers several distinct features, compared to existing liquid handling technologies, including: 1) a fully-automated robotic interface; 2) highly-precise tunable microfluidic dispensing; 3) multi-task operations, including recognizing, capture, positioning, dispensing and releasing; 4) a broad applicability and flexibility for a wide range of biological operations; 5) sample storage in containers with reusable μCD caps for rare or expensive samples. Moreover, the microfluidic cap is ready for mass-production-ready and serves as an inexpensive and disposable platform for various research and development applications.

Supplementary Material

Refer to Web version on PubMed Central for supplementary material.

Acknowledgements

This research has been in part supported by NIH Superfund Research Program at UC Davis (2P42ES004699), NIH NIBIB (1R21EB025938), National Natural Science Foundation of China (31600689), Program for Guangdong Introducing Innovative and Entrepreneurial Teams (2016ZT06D631).The authors would like to acknowledge for the assistance of Baoyue Zhang for valve manifold fabrication, Zhiyu Yang and Dong Chen for 3D components design, Yi Zhang for robot precision evaluation, and Zhuni Chen for nozzle materials selection.

Notes and references

1. Kong F, Yuan L, Zheng YF and Chen W, J. Lab. Autom, 2012, 17, 169–185. [PubMed: 22357568]
2. Oosterbroek RE and van den Berg A, Lab-on-a-Chip: Miniaturized Systems for (Bio) Chemical Analysis and Synthesis, 2003.
3. Harris DC and Jewett MC, Curr. Opin. Biotechnol, 2012, 23, 672–678. [PubMed: 22483202]
4. Villarreal F and Tan C, Front. Chem. Sci. Eng, 2017, 11, 58–65.
5. Villarreal F, Contreras-Llano LE, Chavez M, Ding Y, Fan J, Pan T and Tan C, Nat. Chem. Biol, 2018, 14, 29–35. [PubMed: 29131146]
6. Al-Lazikani B, Banerji U and Workman P, Nat. Biotechnol, 2012, 30, 679–692. [PubMed: 22781697]
7. Beltran H, Beer TM, Carducci MA, De Bono J, Gleave M, Hussain M, Kelly WK, Saad F, Sternberg C, Tagawa ST and Tannock IF, Eur. Urol, 2011, 60, 279–290. [PubMed: 21592649]
8. Art M, Dufey V, Gast U, Gligor I, Koch L and Kubasch R, Nat. Methods, 2016, 1–22.
9. Ding Y, Huang E, Lam KS and Pan T, Lab Chip, 2013, 13, 1902–1910. [PubMed: 23525299]
10. Derby B, J. Mater. Chem, 2008, 18, 5717–5721.
11. Dunn DA and Feygin I, Drug Discov. Today, 2000, 5, S84–S91.
12. Lorenz MGO, J. Lab. Autom, 2004, 9, 262–267.
13. Feature T, Nat. Methods, 2008, 5, 109–112. [PubMed: 18165807]
14. Mathes SH and Parker CN, Requirements of skin tissue models for high-throughput screening, Elsevier Inc, 2017.
15. Mattheakis L, J. Biomol. Screen, 2014, 19, 478–480. [PubMed: 24509067]
16. Scott-brown J and A. Papachristodoulou, 2017, 1–10.
17. Liu C and Tomizuka M, in Proceedings - IEEE International Conference on Robotics and Automation, 2016, vol. 2016-6, pp. 3095–3102.
18. Mitchell HT, Noxon IC, Chaplan CA, Carlton SJ, Liu CH, Ganaja KA, Martinez NW, Immoos CE, Costanzo PJ and Martinez AW, Lab Chip, 2015, 15, 2213–2220. [PubMed: 25851055]
19. O'Connell TN, Ramsay J, Rieth SF, Shapiro MJ and Stroh JG, Anal. Chem, 2014, 86, 7413–7420. [PubMed: 25033415]
20. Fredrickson CK and Fan ZH, Lab Chip, 2004, 4, 526–533. [PubMed: 15570361]
21. Chen A and Pan T, Lab Chip, 2011, 11, 727–732. [PubMed: 21109877]
22. Fan J, Men Y, Hao Tseng K, Ding Y, Ding Y, Villarreal F, Tan C, Li B and Pan T, Biomicrofluidics, 2018, 12, 034107. [PubMed: 29861810]
23. Cheng SX, Li T and Chandra S, J. Mater. Process. Technol, 2005, 159, 295–302.
24. Sirringhaus H, Kawase T, Friend RH, Shimoda T, Inbasekaran M, Wu W and Woo EP, Science (80-.), 2000, 290, 2123–2126.
25. Cooley P, Wallace D and Antohe B, JALA - J. Assoc. Lab. Autom, 2002, 7, 33–39.
26. Jacot-Descombes L, Gullo MR, Cadarso VJ and Brugger J, J. Micromechanics Microengineering, 2012, 22, 074012.
27. Zakir Hossain SM, Luckham RE, Smith AM, Lebert JM, Davies LM, Pelton RH, Filipe CDM and Brennan JD, Anal. Chem, 2009, 81, 5474–5483. [PubMed: 19492815]
28. Yoshioka Y and Jabbour GE, Synth. Met, 2006, 156, 779–783.
29. Oh WK, Kim S, Shin KH, Jang Y, Choi M and Jang J, Talanta, 2013, 105, 333–339. [PubMed: 23598027]
30. Hong S, Hong I, Han A, Seo JY and Namgung J, Forensic Sci. Int, 2015, 257, 403–408. [PubMed: 26555502]
31. Reis N, Ainsley C and Derby B, J. Appl. Phys, 2005, 97, 094903.
32. Di Risio S and Yan N, Macromol. Rapid Commun, 2007, 28, 1934–1940.
33. Alkasir RSJ, Ornatska M and Andreescu S, Anal. Chem, 2012, 84, 9729–9737. [PubMed: 23113670]

34. Brennan-Krohn T, Truelson KA, Smith KP and Kirby JE, J. Antimicrob. Chemother, 2017, 72, 2775–2781. [PubMed: 29091221]
35. Li B, Fan J, Li J, Chu J and Pan T, Biomicrofluidics, 2015, 9, 1–11.
36. Antohe BV and Cooley PW, Methods Mol. Biol, 2007, 381, 299–312. [PubMed: 17984526]
37. Setti L, Fraleoni-Morgera A, Ballarin B, Filippini A, Frascaro D and Piana C, in Biosensors and Bioelectronics, 2005, 20, 2019–2026. [PubMed: 15741071]
38. Fan J, Villarreal F, Weyers B, Ding Y, Tseng KH, Li J, Li B, Tan C and Pan T, Lab Chip, 2017, 17, 2198–2207. [PubMed: 28613297]
39. Cheng S and Chandra S, Exp. Fluids, 2003, 34, 755–762.
40. Choi JH, Lee SK, Lim JM, Yang SM and Yi GR, Lab Chip, 2010, 10,456–461. [PubMed: 20126685]
41. Li J, Carney RP, Liu R, Fan J, Zhao S, Chen Y, Lam KS and Pan T, Anal. Chem, 2018, 90, 5833–5840. [PubMed: 29633611]
42. Li J, Tan W, Xiao W, Carney RP, Men Y, Li Y, Quon G, Ajena Y, Lam KS and Pan T, Anal. Chem, 2018,13969–13977. [PubMed: 30358386]
43. Leung K, Zahn H, Leaver T, Konwar KM, Hanson NW, Page AP, Lo C-C, Chain PS, Hallam SJ and Hansen CL, Proc. Natl. Acad. Sci, 2012, 109, 7665–7670. [PubMed: 22547789]
44. Ding Y, Li J, Xiao W, Xiao K, Lee J, Bhardwaj U, Zhu Z, Digiglio P, Yang G, Lam KS and Pan T, Anal. Chem, 2015, 87, 10166–10171 [PubMed: 26334956]
45. Li J, Zhao S, Yang G, Liu R, Xiao W, Disano P, Lam KS and Pan T, ACS Comb. Sci, 2019, 21, 6–10. [PubMed: 30521316]
46. Choi IH, Kim H, Lee S, Baek S and Kim J, Biomicrofluidics, 2015, 9, 064102.
47. Zhang K, Gao M, Chong Z, Li Y, Han X, Chen R and Qin L, Lab Chip, 2016, 16, 4742–4748. [PubMed: 27841430]
48. Mao Y, Pan Y, Li X, Li B, Chu J and Pan T, Lab Chip, 2018, 18, 2720–2729. [PubMed: 30014071]
49. Sutera SP and Skalak R, Annu. Rev. Fluid Mech, 1993, 25, 1–20.
50. Derby B, Annu. Rev. Mater. Res, 2010, 40, 395–414.
51. Markarian SA and Terzyan AM, J. Chem. Eng. Data, 2007, 52, 1704–1709.
52. Lebel RG and Goring DAI, J. Chem. Eng. Data, 1962, 7, 100–101.
53. Choi IH and Kim J, Micro Nano Syst. Lett, 2016, 4, 1.
54. Zong DM, Cinar S, Shis DL, Josić K, Ott W and Bennett MR, ACS Synth. Biol, 2018, 7,1834–1843. [PubMed: 30040895]
55. Thurgood P, Baratchi S, Szydzik C, Zhu JY, Nahavandi S, Mitchell A and Khoshmanesh K, Sensors Actuators, B Chem, 2018, 274,645–653.
56. Gardner TS, Cantor CR and Collins JJ, Nature, 2000, 403, 339–342. [PubMed: 10659857]
57. Baneyx F, Curr. Opin. Biotechnol, 1999, 10, 411–421. [PubMed: 10508629]

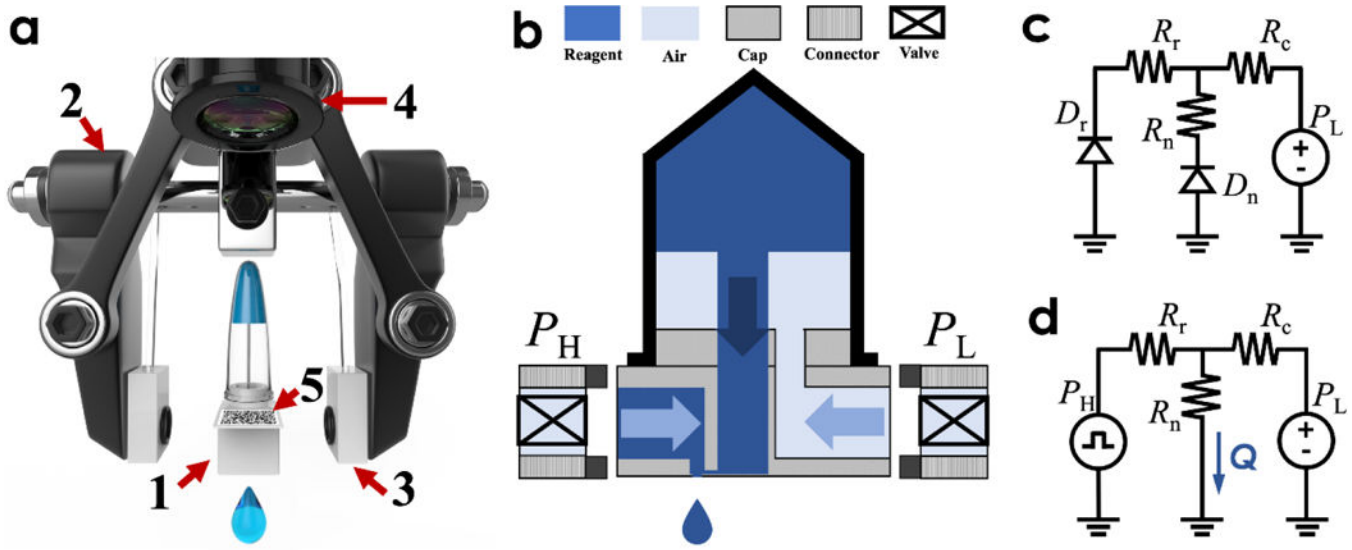

Fig. 1.

a) 3D illustration of the microfluidic Cap-to-Dispense (μCD) system which comprises of essential components: 1) the microfluidic dispensing cap installed on top of the EP tube, 2) the two-finger robotic end-effector equipped with 3) pneumatic controllers, and machine vision module including 4) the camera for recognition of 5) the QR code on the EP tube; b) operational schematic of the microfluidic Cap-to-Dispense (μCD) system; Hydraulic circuits to describe the two states of the droplet dispensing process, namely (c) a loading/refilling state and (d) a dispensing state.

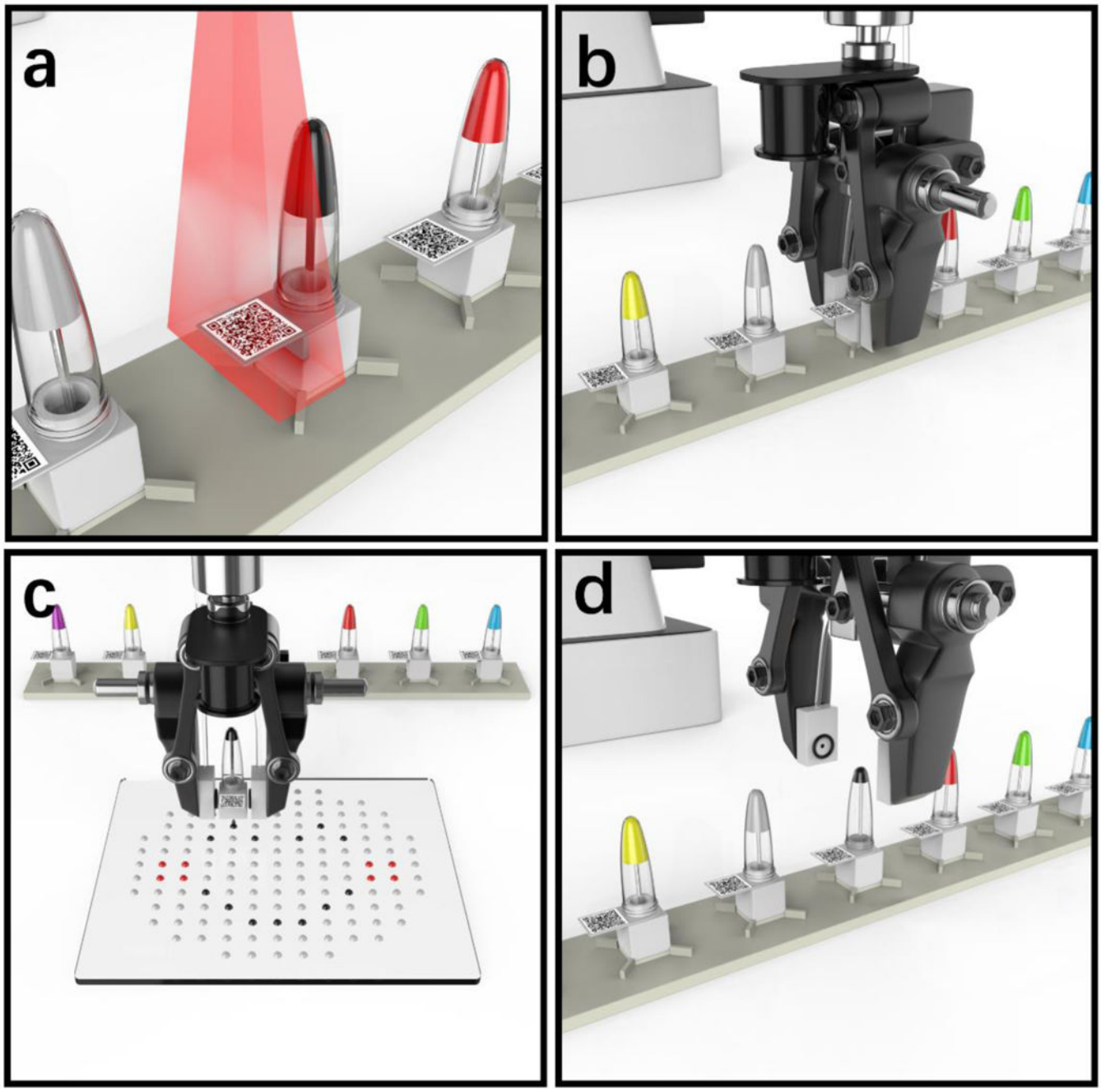

Fig. 2.

Illustration of the complete μCD operation: a) sample recognition; b) catch and positioning; c) dispensing; and d) return and release.

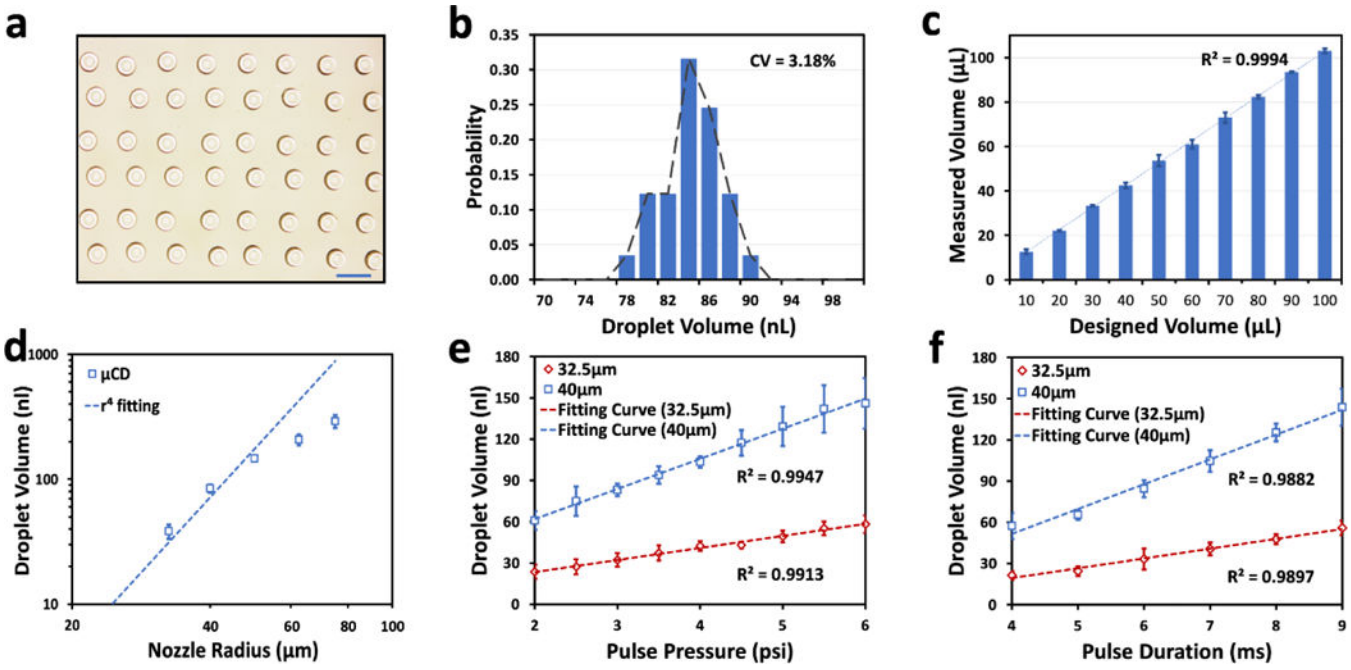

Fig. 3.

a) The microscopic image of droplets array; Scale bar: 1mm; b) The volume distribution of the array; c) Linearity of accumulated droplets from 100 nl to 1000 nl, with a $R^2 > 0.99$; d) The experimental measurements of the ejected droplet volumes depending on multiple nozzle radius, and e) pressure levels, f) pulse durations. In e) and f), the mean droplet volumes are shown in red dots (32.5 µm) and blue dots (40 µm), and all the fitting curves has a $R^2 > 0.98$.

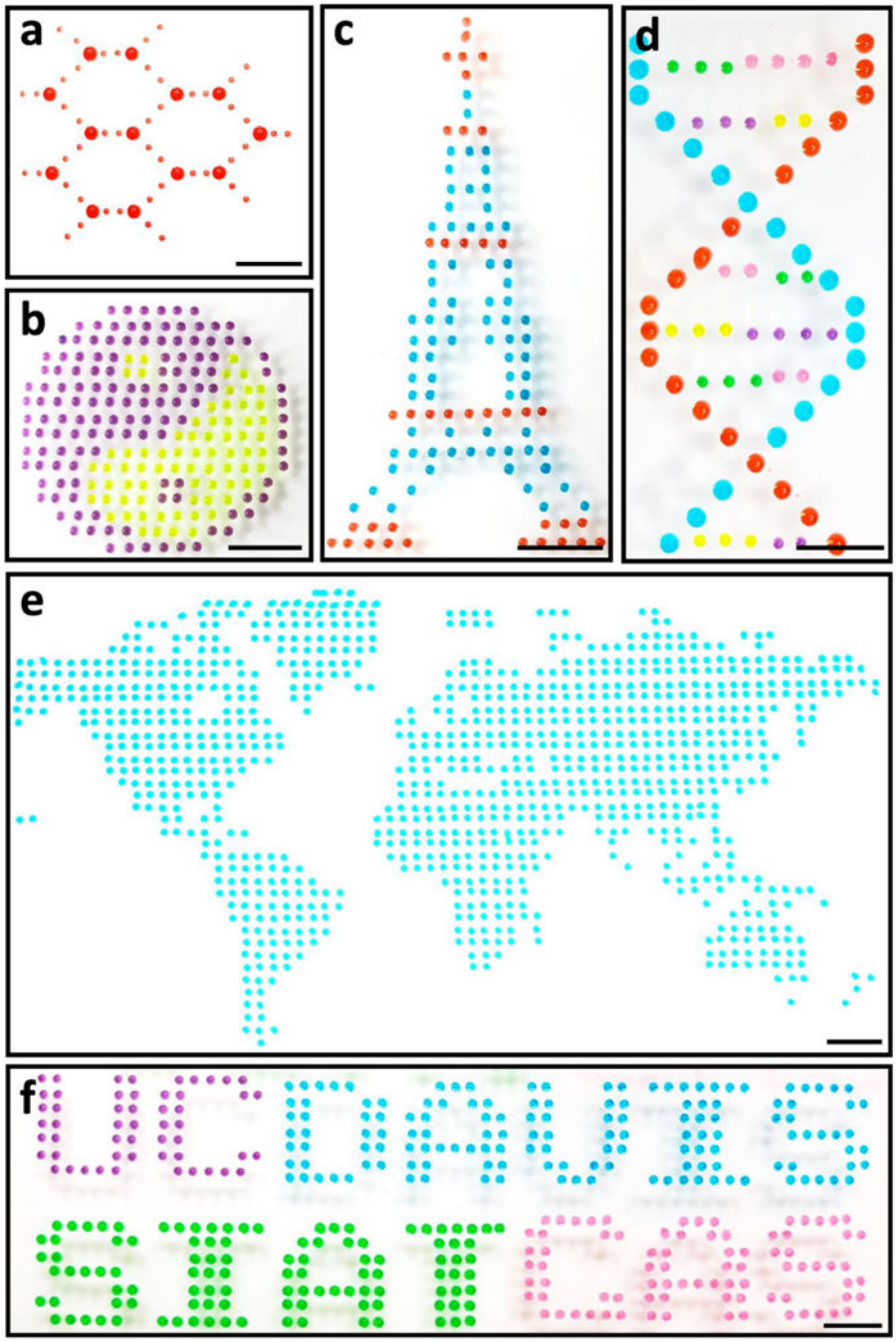

Fig. 4.

Monochrome or multi-colored Droplets-based patterns: a) molecular; b) Taiji; c) Eiffel tower; d) DNA helix; e) world map; and f) UC-DAVIS and SIAT-CAS logos. (scale bar: 5 mm)

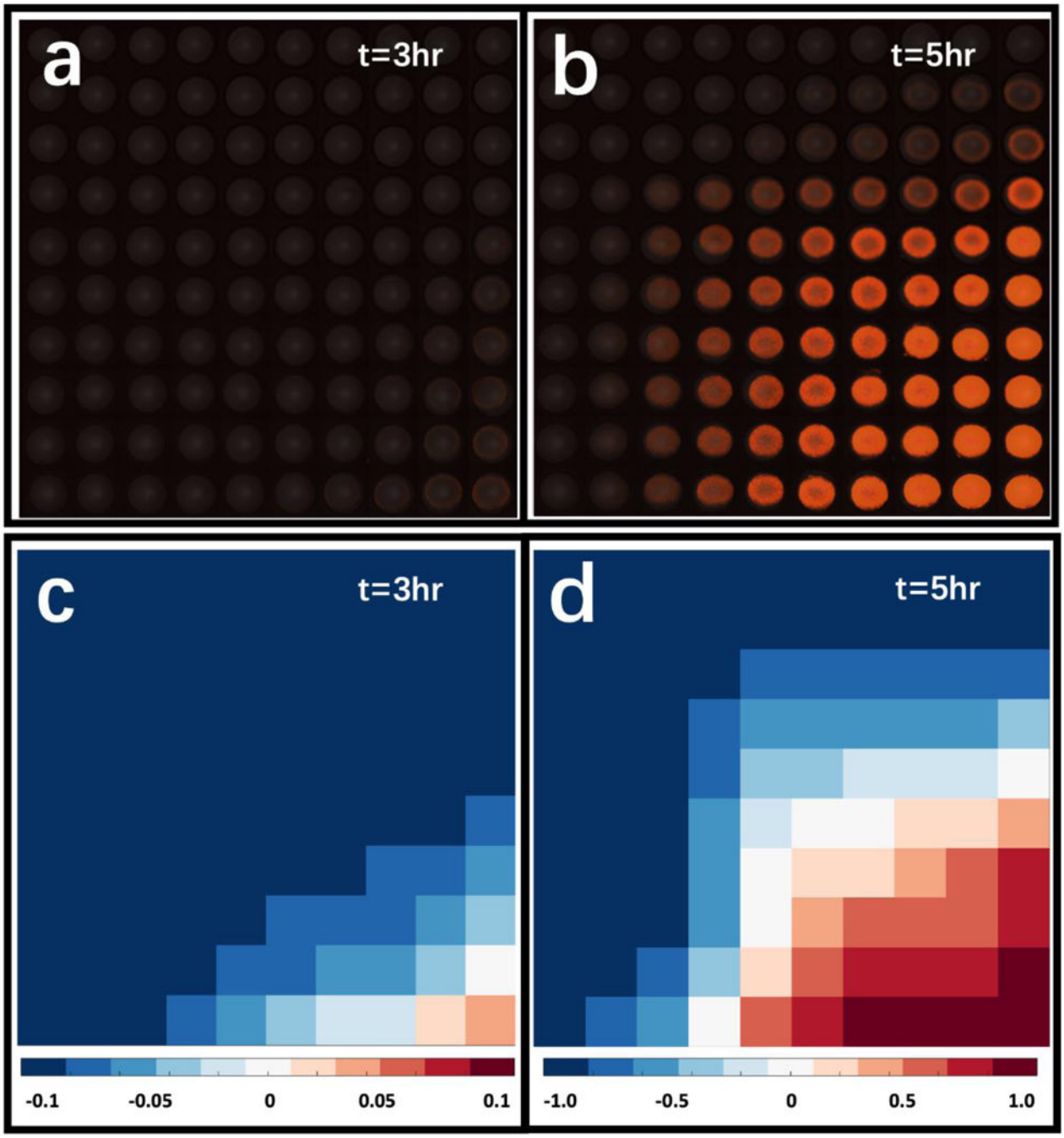

Fig. 5.

The Response of a LacI repressible genetic circuit. a) 3-hr and b) 5-hr results merged by bright field and fluorescent imaging results from the combinatorial droplet array with cell suspension, IPTG, and LB buffer; c) 3-hr and d) 5-hr heat maps analyzed from fluorescent images.